

Detecting High-Energy Neutrinos from Galactic Supernovae with ATLAS

Alex Y. Wen,^{1,*} Carlos A. Argüelles,^{1,†} Ali Kheirandish,^{2,3,‡} and Kohta Murase^{4,5,6,§}

¹*Department of Physics & Laboratory for Particle Physics and Cosmology,
Harvard University, Cambridge, MA 02138, USA*

²*Department of Physics & Astronomy, University of Nevada, Las Vegas, NV 89154, USA*

³*Nevada Center for Astrophysics, University of Nevada, Las Vegas, NV 89154, USA*

⁴*Department of Physics, Department of Astronomy & Astrophysics,
& Center for Multimessenger Astrophysics, Institute for Gravitation and the Cosmos,
The Pennsylvania State University, University Park, PA 16802, USA*

⁵*School of Natural Sciences, Institute for Advanced Study, Princeton, NJ 08540, USA*

⁶*Center for Gravitational Physics and Quantum Information,
Yukawa Institute for Theoretical Physics, Kyoto, Kyoto 16802, Japan*

We show that ATLAS, a collider detector, can measure the flux of high-energy supernova neutrinos, which can be produced from days to months after the explosion. Using Monte Carlo simulations for predicted fluxes, we find at most $\mathcal{O}(0.1 - 1)$ starting events and $\mathcal{O}(10 - 100)$ throughgoing events from a supernova 10 kpc away. Possible Galactic supernovae from Betelgeuse and Eta Carinae are further analyzed as demonstrative examples. We argue that even with limited statistics, ATLAS has the ability to discriminate among flavors and between neutrinos and antineutrinos, making it an unique neutrino observatory so far unmatched in this capability.

INTRODUCTION

The discovery of high-energy astrophysical neutrinos from outside the solar system, first reported by IceCube in 2013 [1, 2], opened a new window to the Universe and marked the start of an era of multimessenger astrophysics with high-energy neutrinos. Cosmic neutrinos are valuable probes of astrophysical processes [3] and neutrino physics [4, 5]. However, small neutrino cross sections [6] and the observed falling energy spectra [7] have so far limited their study to very large volume detectors proposed or built in naturally occurring media such as glaciers [8–10], lakes [11, 12], oceans [13–15], or mountains [16–18]. These detectors are sparser, and have relatively poor energy and angular resolution, and particle identification capabilities, compared to more densely instrumented detectors used in collider and neutrino physics.

Even with limited statistics, IceCube measurements of the astrophysical neutrino flavor composition have already yielded some of the strongest constraints on long-range forces [19], quantum-gravity operators [20, 21], the neutrino lifetime [22–25], and ultralight dark matter interactions [26–28], to name a few of many models [29–31]. Further information can be obtained if astrophysical neutrinos observed are detected by collider detectors, and transient neutrino sources may provide unique opportunities [32–34]. In particular, the next Galactic supernova (SN) has been expected to yield a large detectable neutrino signal not only in the MeV range but also in

the GeV–TeV range, and neutrino detection with large statistics at multienergies is possible [35].

In this *Letter*, we show that large collider detectors serve as a unique astrophysical neutrino telescope, which enables, among other things, the precise measurements of the flavor ratio of astrophysical neutrinos. To demonstrate this, we consider the ATLAS detector [36, 37], a barrel-shaped multi-purpose particle detector situated at the Large Hadron Collider (LHC) at CERN, primarily designed to study reactions originating at a central beam collision point. The sensitive, heavy hadronic (or tile) calorimeter [36, 38–40] is both massive and instrumented, making it a viable fiducial volume for energetic neutrino events to be measured. Moreover, ATLAS also has a sophisticated muon spectrometer [36, 41–44] surrounding the calorimeters, capable of identifying muon tracks and measuring their momenta. This detector combination makes neutrino detection viable.

HIGH-ENERGY NEUTRINO EMISSION FROM SUPERNOVAE

Neutrinos play a critical role in the dynamics of a SN explosion. In addition to the known [45–47] and detected [48, 49] prompt flux of MeV neutrinos, core-collapse SNe have also been predicted to be promising sources of high-energy neutrinos [35]. Recent SN observations especially in the optical band provided strong evidence that interaction with dense, confined circumstellar material (CSM) transiently occurs as the SN shock wave propagates outwards [50–55]. SN remnants (with ages of $10^2 - 10^3$ yr), which are much older, have been established as cosmic-ray accelerators [56, 57]. Interacting SNe can also accelerate cosmic rays, in which they should be efficient sources of high-energy neutrinos and gamma

* alexwen@g.harvard.edu

† carguelles@fas.harvard.edu

‡ ali.kheirandish@unlv.edu

§ murase@psu.edu

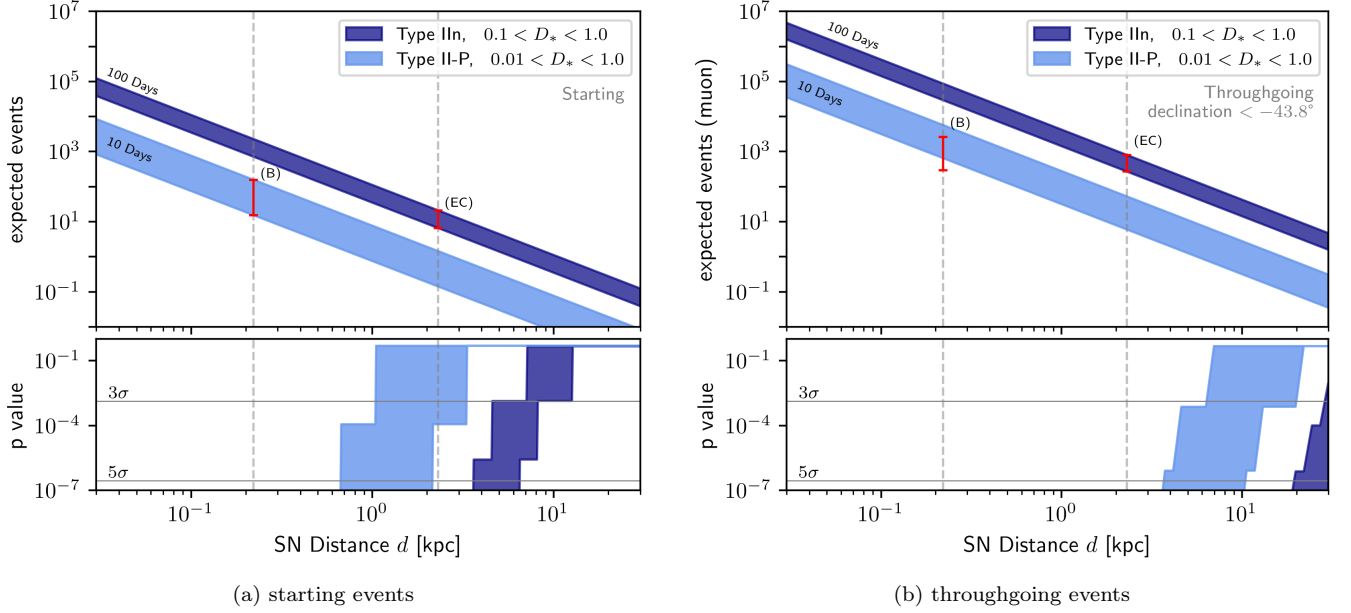


FIG. 1. **Event rates and observation significance of high-energy supernovae neutrinos in ATLAS.** The throughgoing events rates represent the maximum number for a source that is always below the horizon. Below each panel, a plot of p-values for rejecting the atmospheric neutrino background-only hypothesis is shown. The estimated rates for Betelgeuse-like (B) and Eta Carinae-like (EC) SNe scenarios are shown in red bars.

rays [58]. For the next Galactic SN, even ordinary SNe like Type II-P SNe would lead to sufficiently large fluxes of neutrinos that are detectable to many terrestrial neutrino detectors such as IceCube [35], and even mini-bursts from nearby galaxies could be observed [59, 60]. The time window of neutrino signals is predicted to be the 10–100 day time range following an explosion [35].

Type II-P and IIIn SN make up approximately 50% and 3-7%, respectively, of all core-collapse SNe [61]. The result for SNe II-P may also hold for other SN types (II-L, IIb) as long as they have a sufficiently dense CSM [62, 63], so the focus on these two SN types would be representative of the majority of SNe with confined CSM.

We note that predicted neutrino fluxes from SNe have some uncertainties, which primarily depend on CSM properties. The CSM density is written as $\rho_{\text{CS}} = Dr^{-2}$ for a wind-like density profile, where $D \equiv 5 \times 10^{16} \text{ g cm}^{-1} D_*$ is the CSM parameter and r is the radius from the center of the SN explosion. To take into account the impacts, we consider the range of $0.01 < D_* < 1.0$ for SN II-P, and $0.1 < D_* < 1.0$ for SN IIIn. This is sufficient for the purpose of this work to demonstrate the feasibility of ATLAS-like detectors for studies on astrophysical neutrinos, and other parameters such as the spectral index only moderately affect the overall detectability or have degeneracies with D_* . See Refs. [35, 59] for details.

HIGH-ENERGY NEUTRINO EVENTS IN ATLAS

High-energy neutrinos may create signatures as an interaction within the detector itself (*starting* events), or the detection of a muon originating from an interaction within the Earth (*throughgoing* events). For starting events, a charged-current (CC) or neutral-current (NC) deep inelastic scattering (DIS) would leave an energetic hadronic recoil within the ATLAS hadronic calorimeter. A muon, or tau decaying muonically, may instead be detected by the ATLAS muon spectrometer. For throughgoing events, signals can only come from ν_μ CC interactions in surrounding bedrock, with a subdominant contribution from ν_τ (for simplicity, however, the τ component is not taken into account); ATLAS may detect these muons as they traverse the muon spectrometer.

The expected number of starting events induced by neutrinos, \mathcal{N} , in volume of mass m , is given by

$$\mathcal{N} = \int dE_\nu \int dt \dot{\phi}_\nu(E_\nu, t) \sigma_{\nu-\text{nuc}}(E_\nu) N_{\text{nuc}}(m), \quad (1)$$

where $\dot{\phi}_\nu(E_\nu, t) = (dN_\nu/dE_\nu dt)/(4\pi d^2)$ is the all flavor neutrino flux, $dN_\nu/dE_\nu dt$ depends on models (e.g., via D_*), d is the distance to a SN, $\sigma_{\nu-\text{nuc}}(E_\nu)$ is the neutrino-nucleon cross section, and $N_{\text{nuc}}(m)$ is the number of nucleon targets in the fiducial volume.

For high-energy neutrinos, the total cross section $\sigma_{\nu-\text{nuc}}$ is dominated by DIS, and we assume that matter is made of iso-scalar targets. Thus the cross sec-

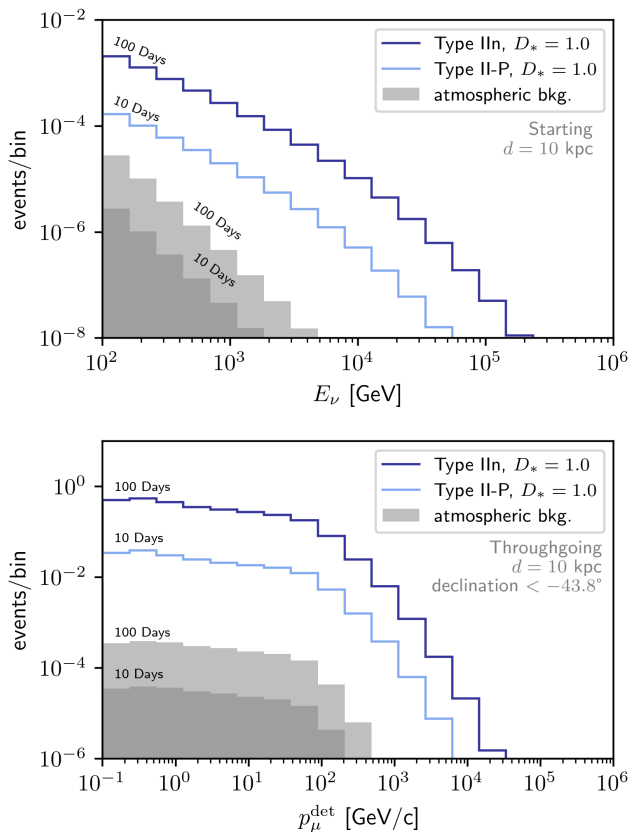


FIG. 2. *Throughgoing and starting event energy distributions.* Top: Neutrino energy E_ν distribution of starting events in ATLAS for Type II-P and II-nc SN with $D_* = 1$ at distance $d = 10$ kpc for 100 (dark blue) and 10 days (light blue) of data taking. Corresponding background from atmospheric neutrinos are shown as shaded gray regions. Bottom: Distribution of the muon momentum, p_μ^{det} , at the detector for throughgoing events. The shape of the spectrum is due to the consideration of 100 GeV neutrino events and above, which produces a flatter distribution of muons at lower energies.

tion is averaged over the neutrino-proton and neutrino-neutron values. The integral in Eq. 1 is taken over the energy range $[10^2, 10^6]$ GeV. We expect the detection of starting events to be analogous to existing ATLAS studies [64, 65] heavily utilizing the missing transverse energy trigger, which is only most efficient above 200 GeV [64, 65]. Therefore, our energy range is chosen to reflect that. At the high-energy end, $E_\nu \dot{\phi}_\nu$ approximately falls with E_ν^{-1} , which yields a negligibly small rate above 10^6 GeV. Indeed for all of the fluxes considered in this work, approximately 90% of all neutrinos are below 10^4 GeV.

The integration over time depends on SN type. We conservatively take 100 days for SNe II-P and 10 days for SNe II-nc, based on the signal-to-background calculation in Ref. [35] as indicative of the characteristic time windows to search for neutrino signals. Finally, neutrinos

and antineutrinos are computed separately owing to their distinct cross sections. For the ATLAS experiment, we assume the hadronic calorimeter mass $m = 4000$ metric tons, and include both CC and NC contributions in $\sigma_{\nu-\text{nuc}}(E_\nu)$ when computing the number of starting events.

Throughgoing events are estimated with a Monte Carlo method using techniques described in Ref. [66]. Neutrino interactions are considered in a rock column of 10 km long preceding the detector. A large number N'_{sim} of ν_μ CC interactions are simulated using *LeptonInjector* [66] as the event generator, using an energy distribution with the shape $\int dt \dot{\phi}_\nu(E_\nu, t) \sigma_{\nu-\text{nuc}}(E_\nu)$ with the appropriate flux, with muon flavor only. Muons with momenta pointing to the detector are propagated through the rock using *PROPOSAL* [67]. The number, n , of muons that are energetic enough to reach the detector are recorded as part of the throughgoing signal. To get the number of expected events, the total number of CC interactions expected in the entire rock column is calculated with Eq. (1) (using only the CC fraction of the total $\sigma_{\nu-\text{nuc}}(E_\nu)$), and scaled with the factor n/N'_{sim} . For more details, see Supplemental Methods and Tables.

The dominant background consists of atmospheric neutrinos. We estimate the background separately for starting and throughgoing events with the same method described above. The atmospheric flux, $\dot{\phi}_{\text{bkg}}$, is obtained using the *NuFlux* [68] interface, which interpolates the neutrino flux computed by *MCEq* [69] assuming the *Hillas-Gaisser H3a* cosmic ray model [70], and the *Sybill12.3c* hadronic interaction model [71]. The solid angle required to calculate the atmospheric flux is based on the conservative angular resolution estimated in Ref. [72], namely 17° for starting events and 5° for throughgoing events, integrated for the same time interval as the corresponding SN.

RESULTS

We evaluate the event rates and the significance of observing high-energy neutrinos from two major representative types of core-collapse SNe (II-P and II-nc) in ATLAS. The expected numbers of signal events varying with distance are shown for starting and throughgoing events in the top panels of Fig. 1. In the bottom panels of Fig. 1, we also show the p-values for rejecting the background-only hypothesis.

Starting events for SNe II-P (II-nc) would only constitute a significant signal if the SN was closer than approximately 0.6 kpc (3 kpc), which is small compared to a ~ 25 kpc size of our Galaxy. However, throughgoing events are produced by a larger effective volume of the target, provided that the source in the sky is below the horizon for a sufficient period of time for neutrinos to interact in the bedrock around the detector. Opti-

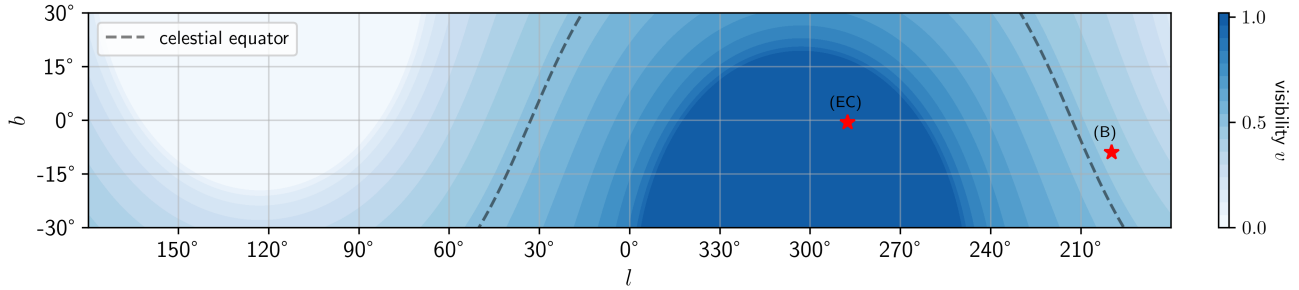


FIG. 3. *Throughgoing events visibility for ATLAS*. Sky map, in Galactic coordinates, showing the visibility, v , of throughgoing events depending on the position in the sky. The locations of Betelgeuse (B) and Eta Carinae (EC) are marked by red stars. The dashed line indicates the celestial equator.

mistically, for a source that is always below the horizon, throughgoing events enable the detection horizon for SNe II-P (IIn) up to around 4 kpc (20 kpc). Cases of the two massive stars Betelgeuse [73–75] and Eta Carinae [76, 77] as prospective Type II-P and IIn SNe are especially intriguing and shown as demonstrative examples, as they are relatively close by to enable a large event rate.

Neutrino energy distributions for starting events at the interaction point for are shown in the top panel of Fig. 2. This spectra adopt the same shape for both starting and throughgoing events, although they would not be measurable for throughgoing events due to muon energy losses. The estimated background caused by atmospheric neutrinos is also shown in the same figure, integrated over both 10 and 100 days to directly compare between the corresponding SN cases.

In addition, we show the muon momentum p_μ^{det} spectrum of throughgoing muons at the detector location in the bottom panel of Fig. 2. The relation between this spectrum to the commonly-measured transverse momentum p_T will depend on the orientation and position of the detector relative to the direction of the incoming neutrino flux; we have assumed that the flux arrives sideways on (perpendicular to the beam axis). The momentum spectrum also gives an idea of the distribution of muon *sagitta* that should be expected in the magnetized part of detector, which will be discussed further in the next section. A key characteristic of this signal is the directionality of the muons, from below the horizon; this would not be produced by cosmic muons, and only a small background is produced by atmospheric muon neutrinos. This background is also shown in Fig. 2 (bottom). With an assumed throughgoing angular resolution of 5° , a signal should be well-correlated to a SN point source.

For the throughgoing events presented in both Fig. 1(b) and 2 (bottom), we have assumed a SN source that is always below the horizon over the course of the 10 or 100 day observation period. However, this will not be the case for every SN event, given that the ATLAS detector, at a latitude of 46.2° , will only see

throughgoing events 100% the time from objects in the celestial sky with a declination of $\delta < -43.8^\circ$. We define the visibility factor, v , of a celestial coordinate to be the fraction of time that it is below the horizon at the ATLAS latitude; hence any object with $\delta < -43.8^\circ$ will have $v = 1$. The value of v will decrease until $\delta > 43.8^\circ$, where $v = 0$. Figure 3 shows the value of v in galactic coordinates; in order to determine an event estimate for throughgoing events, the event number must be multiplied by v .

We also consider a couple of specific cases to illustrate a more concrete scenario of a hypothetical SN explosion. We consider a Betelgeuse-like (B) and a Eta Carinae-like (EC) SN explosion which occur at distances of 0.22 kpc and 2.3 kpc respectively. For (B) and (EC), we use $0.01 < D_* < 1.0$ (assuming a SN II-P) and $0.1 < D_* < 1.0$ (assuming a SN IIn), respectively. The results on these hypothetical signals are indicated in Fig. 1: for (B) we anticipate 15-150 (300-2,600) starting (throughgoing) events, and for (EC) we anticipate 6-21 (170-800) starting (throughgoing) events. The throughgoing signal for (B) is multiplied by a factor of $v = 0.46$ due to its location in the sky, which reduces its time below the horizon. The celestial positions of (B) and (EC) are shown in Fig. 3, mapped to a corresponding visibility v .

DISCUSSION AND CONCLUSION

We demonstrated the feasibility of ATLAS as a unique detector for astrophysical high-energy neutrinos. We also anticipate comparable capabilities for similar detectors like CMS [78]. Any kiloton-scale or larger, densely-instrumented, present or future detector may consider the prospect of detecting high-energy neutrinos from Galactic SNe.

As a previous effort to characterize ATLAS as a viable detector of natural neutrinos, Ref. [72] focused on the precision measurement of atmospheric neutrinos at a lower energy. Although the expected sample size was too small to yield interesting physics, it highlights the

advantages of using a precision collider detector for neutrino physics.

Given ATLAS' unique instrumentation often unseen in dedicated neutrino detectors, it may be possible to discriminate between all three neutrino flavors. Consider a benchmark scenario with 88 (22 NC and 66 CC) starting events, which is roughly the expected signal from (B) with $D_* = 0.1$. We can broadly consider three distinguishable signal channels: (1) one hadronic shower, (2) one hadronic shower plus muon, and (3) two hadronic showers. Each flavor of starting events will contribute to these channels in varying amounts, allowing us to estimate the expected signal in each channel and infer the flavor ratio (f_e, f_μ, f_τ). In Fig. 4 we show the allowed flavor ratios when assuming a (1, 1, 1) ratio flavor composition at Earth. In the same figure, we also show a more pessimistic 2-channel case assuming no sensitivity to channel (3) events. Such a flavor ratio measurement is expected to be of comparable or better performance to current measurements by dedicated experiments [24, 79]. A better understanding of the detector efficiency for throughgoing muons is required to incorporate throughgoing signal (muon-flavor only) into the flavor ratio measurement.

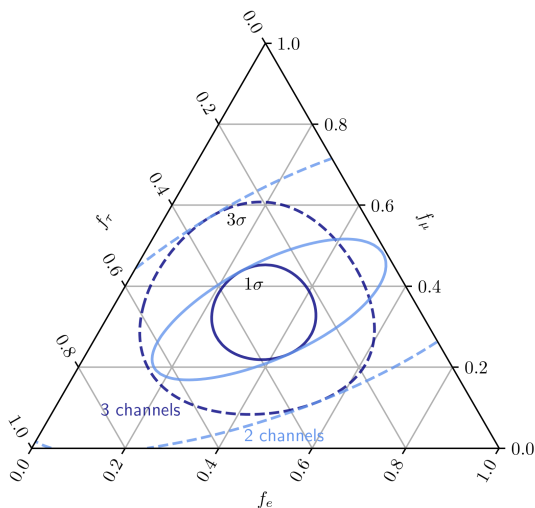


FIG. 4. **Expected flavor triangle allowed region by ATLAS.** The flavor triangle measured at Earth by ATLAS using only starting events from a single close by SN explosion, similar to Betelgeuse (B). The dark blue lines correspond to performing an analysis using all 3 signal channels described in the text, whereas the light blue lines only use channels (1) and (2). Solid and dashed lines indicate 1σ and 3σ significance, respectively.

Another advantage of ATLAS is a superior energy resolution compared to that of larger, dedicated neutrino detectors. The ATLAS hadronic calorimeter energy resolution for jet events is approximately given by $\sigma/E = 50\%/\sqrt{E/\text{GeV}} \oplus 3\%$ [39], translating to approximately $1.6\% \oplus 3\%$ at 1 TeV. This can be contrasted to,

for example, the IceCube energy resolution of $\sim 15\%$ for shower events [80], around an order of magnitude worse.

Finally, ATLAS is expected to have the capability for neutrino-to-antineutrino separation. Assuming a typical path length of around 5 m through the ATLAS muon spectrometer barrel region, which is magnetized at approximately 0.5 T, a 1 TeV muon track will have a sagitta of approximately $500\mu\text{m}$ [81], well above the $\sim 30\text{--}40\mu\text{m}$ muon spectrometer alignment accuracy and the $\sim 80\text{--}90\mu\text{m}$ detector single hit resolution quoted in Refs. [41, 81]. Only at approximately 5 TeV will the sagitta approach $\sim 100\mu\text{m}$, a length scale limited by the detector and alignment resolutions. Since the bulk of muons from both starting and throughgoing events are expected to be less energetic, it is likely that ATLAS hardware can determine the charge of most muons that traverse it. If successful, ATLAS might be the only neutrino detector that can measure the ratio of neutrinos to antineutrinos, which can be used to discriminate between different production mechanisms at the source.

In conclusion, the event rates and estimated hardware capabilities of ATLAS make it a promising high-energy neutrino telescope. We hope that our findings spur the development of new triggers and analyses to enable a precise measurement of the next nearby SN event.

ACKNOWLEDGEMENTS

We thank Austin Schneider and Nicholas Kamp for their help with **LeptonInjector**. We thank Masahiro Morii and Melissa Franklin for insightful discussions about the capabilities of ATLAS. We thank the KITP for being an engaging space to work on physics, and this research was supported in part by the National Science Foundation under Grants No. NSF PHY-1748958 and PHY-2309135. CAA is supported by the Faculty of Arts and Sciences of Harvard University and the Alfred P. Sloan Foundation. AK is supported by the NASA Grant 80NSSC23M0104. AYW is supported by the Harvard Physics Department Purcell Fellowship and the Natural Sciences and Engineering Research Council of Canada (NSERC), funding reference number PGSD-577971-2023. KM is supported by the NSF Grant No. AST-2108466 and No. AST-2108467, and KAKENHI No. 20H01901 and No. 20H05852.

-
- [1] M. G. Aartsen *et al.* (IceCube), First observation of PeV-energy neutrinos with IceCube, *Phys. Rev. Lett.* **111**, 021103 (2013), [arXiv:1304.5356 \[astro-ph.HE\]](#).
- [2] M. G. Aartsen *et al.* (IceCube), Evidence for High-Energy Extraterrestrial Neutrinos at the IceCube Detector, *Science* **342**, 1242856 (2013), [arXiv:1311.5238 \[astro-ph.HE\]](#).
- [3] M. Ackermann *et al.*, Astrophysics Uniquely Enabled by Observations of High-Energy Cosmic Neutrinos, *Bull. Am. Astron. Soc.* **51**, 185 (2019), [arXiv:1903.04334 \[astro-ph.HE\]](#).
- [4] C. A. Argüelles, M. Bustamante, A. Kheirandish, S. Palomares-Ruiz, J. Salvado, and A. C. Vincent, Fundamental physics with high-energy cosmic neutrinos today and in the future, *PoS ICRC2019*, 849 (2020), [arXiv:1907.08690 \[astro-ph.HE\]](#).
- [5] M. Ackermann *et al.*, High-energy and ultra-high-energy neutrinos: A Snowmass white paper, *JHEAp* **36**, 55 (2022), [arXiv:2203.08096 \[hep-ph\]](#).
- [6] J. A. Formaggio and G. P. Zeller, From eV to EeV: Neutrino Cross Sections Across Energy Scales, *Rev. Mod. Phys.* **84**, 1307 (2012), [arXiv:1305.7513 \[hep-ex\]](#).
- [7] R. Abbasi *et al.* (IceCube), The IceCube high-energy starting event sample: Description and flux characterization with 7.5 years of data, *Phys. Rev. D* **104**, 022002 (2021), [arXiv:2011.03545 \[astro-ph.HE\]](#).
- [8] P. W. Gorham *et al.* (ANITA), Characteristics of Four Upward-pointing Cosmic-ray-like Events Observed with ANITA, *Phys. Rev. Lett.* **117**, 071101 (2016), [arXiv:1603.05218 \[astro-ph.HE\]](#).
- [9] P. W. Gorham *et al.* (ANITA), Observation of an Unusual Upward-going Cosmic-ray-like Event in the Third Flight of ANITA, *Phys. Rev. Lett.* **121**, 161102 (2018), [arXiv:1803.05088 \[astro-ph.HE\]](#).
- [10] M. G. Aartsen *et al.* (IceCube-Gen2), IceCube-Gen2: the window to the extreme Universe, *J. Phys. G* **48**, 060501 (2021), [arXiv:2008.04323 \[astro-ph.HE\]](#).
- [11] A. D. Avrorin *et al.* (BAIKAL), A search for neutrino signal from dark matter annihilation in the center of the Milky Way with Baikal NT200, *Astropart. Phys.* **81**, 12 (2016), [arXiv:1512.01198 \[astro-ph.HE\]](#).
- [12] A. D. Avrorin *et al.*, Status and recent results of the BAIKAL-GVD project, *Phys. Part. Nucl.* **46**, 211 (2015).
- [13] S. Adrian-Martinez *et al.* (KM3Net), Letter of intent for KM3NeT 2.0, *J. Phys. G* **43**, 084001 (2016), [arXiv:1601.07459 \[astro-ph.IM\]](#).
- [14] M. Agostini *et al.* (P-ONE), The Pacific Ocean Neutrino Experiment, *Nature Astron.* **4**, 913 (2020), [arXiv:2005.09493 \[astro-ph.HE\]](#).
- [15] Z. P. Ye *et al.*, Proposal for a neutrino telescope in South China Sea, (2022), [arXiv:2207.04519 \[astro-ph.HE\]](#).
- [16] M. Sasaki and T. Kifune, Ashra Neutrino Telescope Array (NTA): Combined Imaging Observation of Astroparticles — For Clear Identification of Cosmic Accelerators and Fundamental Physics Using Cosmic Beams —, *JPS Conf. Proc.* **15**, 011013 (2017).
- [17] A. M. Brown, M. Bagheri, M. Doro, E. Gazda, D. Kieda, C. Lin, Y. Onel, N. Otte, I. Taboada, and A. Wang, Trinity: An Imaging Air Cherenkov Telescope to Search for Ultra-High-Energy Neutrinos, in *37th International Cosmic Ray Conference* (2021) [arXiv:2109.03125 \[astro-ph.IM\]](#).
- [18] W. G. Thompson (TAMBO), TAMBO: Searching for Tau Neutrinos in the Peruvian Andes (2023) [arXiv:2308.09753 \[astro-ph.HE\]](#).
- [19] M. Bustamante and S. K. Agarwalla, Universe’s Worth of Electrons to Probe Long-Range Interactions of High-Energy Astrophysical Neutrinos, *Phys. Rev. Lett.* **122**, 061103 (2019), [arXiv:1808.02042 \[astro-ph.HE\]](#).
- [20] C. A. Argüelles, T. Katori, and J. Salvado, New Physics in Astrophysical Neutrino Flavor, *Phys. Rev. Lett.* **115**, 161303 (2015), [arXiv:1506.02043 \[hep-ph\]](#).
- [21] R. Abbasi *et al.* (IceCube), Search for quantum gravity using astrophysical neutrino flavour with IceCube, *Nature Phys.* **18**, 1287 (2022), [arXiv:2111.04654 \[hep-ex\]](#).
- [22] I. M. Shoemaker and K. Murase, Probing BSM Neutrino Physics with Flavor and Spectral Distortions: Prospects for Future High-Energy Neutrino Telescopes, *Phys. Rev. D* **93**, 085004 (2016), [arXiv:1512.07228 \[astro-ph.HE\]](#).
- [23] M. Bustamante, J. F. Beacom, and K. Murase, Testing decay of astrophysical neutrinos with incomplete information, *Phys. Rev. D* **95**, 063013 (2017), [arXiv:1610.02096 \[astro-ph.HE\]](#).
- [24] N. Song, S. W. Li, C. A. Argüelles, M. Bustamante, and A. C. Vincent, The Future of High-Energy Astrophysical Neutrino Flavor Measurements, *JCAP* **04**, 054, [arXiv:2012.12893 \[hep-ph\]](#).
- [25] A. Abdullahi and P. B. Denton, Visible Decay of Astrophysical Neutrinos at IceCube, *Phys. Rev. D* **102**, 023018 (2020), [arXiv:2005.07200 \[hep-ph\]](#).
- [26] Y. Farzan and S. Palomares-Ruiz, Flavor of cosmic neutrinos preserved by ultralight dark matter, *Phys. Rev. D* **99**, 051702 (2019), [arXiv:1810.00892 \[hep-ph\]](#).
- [27] M. M. Reynoso, O. A. Sampayo, and A. M. Carulli, Neutrino interactions with ultralight axion-like dark matter, *Eur. Phys. J. C* **82**, 274 (2022), [arXiv:2203.11642 \[hep-ph\]](#).
- [28] C. A. Argüelles, K. Farrag, and T. Katori, Ultralight Dark Matter Limits from Astrophysical Neutrino Flavour, *PoS ICRC2023*, 1415 (2023).
- [29] C. A. Argüelles, K. Farrag, T. Katori, R. Khandelwal, S. Mandalia, and J. Salvado, Sterile neutrinos in astrophysical neutrino flavor, *JCAP* **02**, 015, [arXiv:1909.05341 \[hep-ph\]](#).
- [30] K. Carloni, C. A. Argüelles, I. Martinez-Soler, K. S. Babu, and P. S. B. Dev, Probing Pseudo-Dirac Neutrinos with Astrophysical Sources at IceCube, *PoS ICRC2023*, 1040 (2023), [arXiv:2212.00737 \[astro-ph.HE\]](#).
- [31] C. A. Argüelles *et al.*, Snowmass white paper: beyond the standard model effects on neutrino flavor: Submitted to the proceedings of the US community study on the future of particle physics (Snowmass 2021), *Eur. Phys. J. C* **83**, 15 (2023), [arXiv:2203.10811 \[hep-ph\]](#).
- [32] K. Murase and I. M. Shoemaker, Neutrino Echoes from Multimessenger Transient Sources, *Phys. Rev. Lett.* **123**, 241102 (2019), [arXiv:1903.08607 \[hep-ph\]](#).
- [33] K. Murase and I. Bartos, High-Energy Multimessenger Transient Astrophysics, *Ann. Rev. Nucl. Part. Sci.* **69**, 477 (2019), [arXiv:1907.12506 \[astro-ph.HE\]](#).
- [34] C. Guépin, K. Kotera, and F. Oikonomou, High-energy neutrino transients and the future of multimessenger astronomy, *Nature Rev. Phys.* **4**, 697 (2022), [arXiv:2207.12205 \[astro-ph.HE\]](#).
- [35] K. Murase, New Prospects for Detecting High-Energy Neutrinos from Nearby Supernovae, *Phys. Rev. D* **97**,

- 081301 (2018), [arXiv:1705.04750 \[astro-ph.HE\]](#).
- [36] G. Aad *et al.* (ATLAS), The ATLAS Experiment at the CERN Large Hadron Collider, *JINST* **3**, S08003.
- [37] G. Aad *et al.* (ATLAS), The ATLAS Experiment at the CERN Large Hadron Collider: A Description of the Detector Configuration for Run 3, (2023), [arXiv:2305.16623 \[physics.ins-det\]](#).
- [38] ATLAS tile calorimeter: Technical design report, (1996).
- [39] M. Aaboud *et al.* (ATLAS), Operation and performance of the ATLAS Tile Calorimeter in Run 1, *Eur. Phys. J. C* **78**, 987 (2018), [arXiv:1806.02129 \[hep-ex\]](#).
- [40] G. Aad *et al.* (ATLAS), Jet energy scale and resolution measured in proton-proton collisions at $\sqrt{s} = 13$ TeV with the ATLAS detector, *Eur. Phys. J. C* **81**, 689 (2021), [arXiv:2007.02645 \[hep-ex\]](#).
- [41] G. Aad *et al.* (ATLAS), Muon reconstruction performance of the ATLAS detector in proton-proton collision data at $\sqrt{s} = 13$ TeV, *Eur. Phys. J. C* **76**, 292 (2016), [arXiv:1603.05598 \[hep-ex\]](#).
- [42] G. Aad *et al.* (ATLAS), Muon reconstruction and identification efficiency in ATLAS using the full Run 2 *pp* collision data set at $\sqrt{s} = 13$ TeV, *Eur. Phys. J. C* **81**, 578 (2021), [arXiv:2012.00578 \[hep-ex\]](#).
- [43] G. Aad *et al.* (ATLAS), Commissioning of the ATLAS Muon Spectrometer with Cosmic Rays, *Eur. Phys. J. C* **70**, 875 (2010), [arXiv:1006.4384 \[physics.ins-det\]](#).
- [44] ATLAS muon spectrometer: Technical design report, (1997).
- [45] H. T. Janka, Neutrino Emission from Supernovae [10.1007/978-3-319-21846-5-4](#) (2017), [arXiv:1702.08713 \[astro-ph.HE\]](#).
- [46] H. A. Bethe, Supernova mechanisms, *Rev. Mod. Phys.* **62**, 801 (1990).
- [47] S. E. Woosley, A. Heger, and T. A. Weaver, The evolution and explosion of massive stars, *Rev. Mod. Phys.* **74**, 1015 (2002).
- [48] K. Hirata *et al.* (Kamiokande-II), Observation of a Neutrino Burst from the Supernova SN 1987a, *Phys. Rev. Lett.* **58**, 1490 (1987).
- [49] R. M. Bionta *et al.*, Observation of a Neutrino Burst in Coincidence with Supernova SN 1987a in the Large Magellanic Cloud, *Phys. Rev. Lett.* **58**, 1494 (1987).
- [50] O. Yaron *et al.*, Confined Dense Circumstellar Material Surrounding a Regular Type II Supernova: The Unique Flash-Spectroscopy Event of SN 2013fs, *Nature Phys.* **13**, 510 (2017), [arXiv:1701.02596 \[astro-ph.HE\]](#).
- [51] V. Morozova, A. L. Piro, and S. Valenti, Measuring the Progenitor Masses and Dense Circumstellar Material of Type II Supernovae, *Astrophys. J.* **858**, 15 (2018), [arXiv:1709.04928 \[astro-ph.HE\]](#).
- [52] G. Hosseinzadeh *et al.*, Short-Lived Circumstellar Interaction in the Low-Luminosity Type IIP SN 2016bkv, *Astrophys. J.* **861**, 63 (2018), [arXiv:1801.00015 \[astro-ph.HE\]](#).
- [53] I. Boian and J. H. Groh, Progenitors of early-time interacting supernovae, *MNRAS* **496**, 1325 (2020), [arXiv:2001.07651 \[astro-ph.SR\]](#).
- [54] S. Tinyanont *et al.*, Progenitor and close-in circumstellar medium of type II supernova 2020fqv from high-cadence photometry and ultra-rapid UV spectroscopy, *Mon. Not. Roy. Astron. Soc.* **512**, 2777 (2022), [arXiv:2110.10742 \[astro-ph.SR\]](#).
- [55] K. A. Bostroem *et al.*, Early Spectroscopy and Dense Circumstellar Medium Interaction in SN2023ixf, (2023), [arXiv:2306.10119 \[astro-ph.HE\]](#).
- [56] S. Funk, Ground- and Space-Based Gamma-Ray Astronomy, *Ann. Rev. Nucl. Part. Sci.* **65**, 245 (2015), [arXiv:1508.05190 \[astro-ph.HE\]](#).
- [57] D. Caprioli, Cosmic-ray Acceleration and Propagation, *PoS ICRC2015*, 008 (2016), [arXiv:1510.07042 \[astro-ph.HE\]](#).
- [58] K. Murase, T. A. Thompson, B. C. Lacki, and J. F. Beacom, New Class of High-Energy Transients from Crashes of Supernova Ejecta with Massive Circumstellar Material Shells, *Phys. Rev. D* **84**, 043003 (2011), [arXiv:1012.2834 \[astro-ph.HE\]](#).
- [59] A. Kheirandish and K. Murase, Detecting High-Energy Neutrino Minibursts from Local Supernovae with Multiple Neutrino Observatories, (2022), [arXiv:2204.08518 \[astro-ph.HE\]](#).
- [60] N. Valtonen-Mattila and E. O'Sullivan, Prospects for Extending the Core-collapse Supernova Detection Horizon Using High-energy Neutrinos, *Astrophys. J.* **945**, 98 (2023), [arXiv:2206.00450 \[astro-ph.HE\]](#).
- [61] O. Graur, F. B. Bianco, M. Modjaz, I. Shivvers, A. V. Filippenko, W. Li, and N. Smith, LOSS Revisited - II: The relative rates of different types of supernovae vary between low- and high-mass galaxies, *Astrophys. J.* **837**, 121 (2017), [arXiv:1609.02923 \[astro-ph.HE\]](#).
- [62] R. Margutti *et al.*, Ejection of the Massive Hydrogen-rich Envelope Time with the Collapse of the Stripped SN 2014C, *Astrophys. J.* **835**, 140 (2017), [arXiv:1601.06806 \[astro-ph.HE\]](#).
- [63] K. Murase, A. Franckowiak, K. Maeda, R. Margutti, and J. F. Beacom, High-Energy Emission from Interacting Supernovae: New Constraints on Cosmic-Ray Acceleration in Dense Circumstellar Environments, *Astrophys. J.* **874**, 80 (2019), [arXiv:1807.01460 \[astro-ph.HE\]](#).
- [64] G. Aad *et al.* (ATLAS), Search for new phenomena in events with an energetic jet and missing transverse momentum in *pp* collisions at $\sqrt{s} = 13$ TeV with the ATLAS detector, *Phys. Rev. D* **103**, 112006 (2021), [arXiv:2102.10874 \[hep-ex\]](#).
- [65] E. Pompa Pacchi (ATLAS), Constraining the Dark Sector with the Mono-jet signature with the ATLAS detector at the LHC, *PoS LHCP2021*, 254 (2021).
- [66] R. Abbasi *et al.* (IceCube), LeptonInjector and LeptonWeighter: A neutrino event generator and weighter for neutrino observatories, *Comput. Phys. Commun.* **266**, 108018 (2021), [arXiv:2012.10449 \[physics.comp-ph\]](#).
- [67] J. H. Koehne, K. Frantzen, M. Schmitz, T. Fuchs, W. Rhode, D. Chirkin, and J. Becker Tjus, PROPOSAL: A tool for propagation of charged leptons, *Comput. Phys. Commun.* **184**, 2070 (2013).
- [68] IceCube, Nuflux code, <https://github.com/icecube/nuflux> (2023).
- [69] A. Fedynitch and M. Huber, Data-driven hadronic interaction model for atmospheric lepton flux calculations, *Phys. Rev. D* **106**, 083018 (2022), [arXiv:2205.14766 \[astro-ph.HE\]](#).
- [70] T. K. Gaisser, T. Stanev, and S. Tilav, Cosmic Ray Energy Spectrum from Measurements of Air Showers, *Front. Phys. (Beijing)* **8**, 748 (2013), [arXiv:1303.3565 \[astro-ph.HE\]](#).
- [71] F. Riehn, H. P. Dembinski, R. Engel, A. Fedynitch, T. K. Gaisser, and T. Stanev, The hadronic interaction model SIBYLL 2.3c and Feynman scaling, *PoS ICRC2017*, 301 (2018), [arXiv:1709.07227 \[hep-ph\]](#).

- [72] J. Kopp and M. Lindner, Detecting atmospheric neutrino oscillations in the ATLAS detector at CERN, *Phys. Rev. D* **76**, 093003 (2007), [arXiv:0705.2595 \[hep-ph\]](#).
- [73] M. M. Dolan, G. J. Mathews, D. D. Lam, N. Q. Lan, G. J. Herczeg, and D. S. P. Dearborn, Evolutionary tracks for betelgeuse, *The Astrophysical Journal* **819**, 7 (2016).
- [74] N. Smith, K. H. Hinkle, and N. Ryde, Red supergiants as potential Type II_n supernova progenitors: Spatially resolved 4.6 micron CO emission around VY CMa and Betelgeuse, *Astron. J.* **137**, 3558 (2009), [arXiv:0811.3037 \[astro-ph\]](#).
- [75] G. Meynet, L. Haemmerle, S. Ekstrom, C. Georgy, J. Groh, and A. Maeder, The past and future evolution of a star like Betelgeuse, *EAS Publ. Ser.* **60**, 17 (2013), [arXiv:1303.1339 \[astro-ph.SR\]](#).
- [76] N. Smith, A Blast Wave from the 1843 Eruption of Eta Carinae, *Nature* **455**, 201 (2008), [arXiv:0809.1678 \[astro-ph\]](#).
- [77] N. Smith, A Model for the 19th Century Eruption of Eta Carinae: CSM Interaction Like a Scaled-Down Type II_n Supernova, *Mon. Not. Roy. Astron. Soc.* **429**, 2366 (2013), [arXiv:1209.6155 \[astro-ph.SR\]](#).
- [78] S. Chatrchyan *et al.* (CMS), The CMS Experiment at the CERN LHC, *JINST* **3**, S08004.
- [79] R. Abbasi *et al.* (IceCube), Detection of astrophysical tau neutrino candidates in IceCube, *Eur. Phys. J. C* **82**, 1031 (2022), [arXiv:2011.03561 \[hep-ex\]](#).
- [80] M. G. Aartsen *et al.* (IceCube), Energy Reconstruction Methods in the IceCube Neutrino Telescope, *JINST* **9**, P03009, [arXiv:1311.4767 \[physics.ins-det\]](#).
- [81] Technical Design Report for the Phase-II Upgrade of the ATLAS Muon Spectrometer, .
- [82] Procedure for the LHC Higgs boson search combination in Summer 2011, (2011).
- [83] M. C. Gonzalez-Garcia, F. Halzen, and V. Niro, Reevaluation of the Prospect of Observing Neutrinos from Galactic Sources in the Light of Recent Results in Gamma Ray and Neutrino Astronomy, *Astropart. Phys.* **57-58**, 39 (2014), [arXiv:1310.7194 \[astro-ph.HE\]](#).
- [84] F. Halzen, A. Kheirandish, and V. Niro, Prospects for Detecting Galactic Sources of Cosmic Neutrinos with IceCube: An Update, *Astropart. Phys.* **86**, 46 (2017), [arXiv:1609.03072 \[astro-ph.HE\]](#).
- [85] P. A. Zyla *et al.* (Particle Data Group), Review of Particle Physics, *PTEP* **2020**, 083C01 (2020).
- [86] A. C. Vincent, C. A. Argüelles, and A. Kheirandish, High-energy neutrino attenuation in the Earth and its associated uncertainties, *JCAP* **11**, 012, [arXiv:1706.09895 \[hep-ph\]](#).

Supplemental Methods and Tables

Sensitivity to flavor ratio

While the hadronic calorimeter has demonstrated ability to detect lepton tracks [42], the energy deposit per length is still small, and is relatively unstudied at energies considered in this work; hence to be conservative, we assume the hadronic calorimeter is only sensitive to hadronic showers caused by nuclear recoils from CC or NC interactions, with a perfect efficiency. We assume this efficiency is one, or at least close to one, since we do not require sophisticated reconstruction of particles, but only a large energy deposit in a localized region.

For μ -flavor events, we will assume an overall muon spectrometer efficiency of $\varepsilon_\mu = 0.75$, approximately the reconstruction and selection efficiency at 0.5-1 TeV for high- p_T working point muons reported in Ref. [42]. The detection of muons is expected to rely only on the muon spectrometer, and not the inner detector which is also used to reconstruct tracks during normal detector operation.

Finally, for τ -flavor events we assume that we can only detect a hadronic τ decay if it propagates 0.5 m or less - corresponding to an energy of less than $\sim 10^4$ GeV which includes around $\varepsilon_{\tau \text{ range}} = 90\%$ of all τ events produced in all SN scenarios considered. If the τ decays into a muon or electron, we assume the signal is indistinguishable from a e or μ -flavor event.

Thus we identify three possible signal channels: (1) only a hadronic shower, from NC, ν_e , and $\tau \rightarrow e$ events; (2) a hadronic shower and a muon, from mostly ν_μ and $\tau \rightarrow \mu$ events; and (3) two hadronic showers separated by some distance, caused by hadronic τ events. These signal channels are summarized in Suppl. Table I. Each flavor of starting event will contribute to these channels in varying amounts, taking into account the estimated detector efficiencies. This allows us to infer the flavor ratio.

To estimate the discovery p-value of rejecting a $(f_e, f_\mu, f_\tau) = (1, 1, 1)$ null hypothesis, we employ a similar test used in Refs. [59, 82–84]. We define the test statistic

$$q_0 = -2 \log \mathcal{L} = 2 \sum_i \left(Y_i - N_i + N_i \log \left(\frac{N_i}{Y_i} \right) \right), \quad (\text{A1})$$

where i runs over each channel as summarized in Suppl. Table I. Y_i and N_i are the expected number of events given a $(1, 1, 1)$ and varying (f_e, f_μ, f_τ) ratio, respectively. The test statistic value corresponding to 1σ , 3σ p-values is looked up in the table for the joint estimation of two parameters in chapter 40 of the Review of Particle Physics [85].

Calculation of discovery p-value

The discovery p-value of rejecting the background hypothesis for starting and throughgoing events presented in Fig. 1 is calculated in the same way as in Refs. [59, 82–84]. The test statistic is again given by Eq. (A1) where Y_i and N_i are the expected number of events calculated with the background only hypothesis and background-plus-signal hypothesis, respectively. Due to the possible smallness of the signal, i only runs over one bin which contains all the events. The p-value p is given by

$$p = \frac{1}{2} \left(1 - \text{erf} \left(\sqrt{\frac{q_0}{2}} \right) \right). \quad (\text{A2})$$

SUPPL. TABLE I. A summary of the three starting event signal channels that may be used for flavor measurements. N_{NC} NC and N_{CC} CC events, required for estimating the event number in each channel, are estimated using the methods described in the text for starting events.

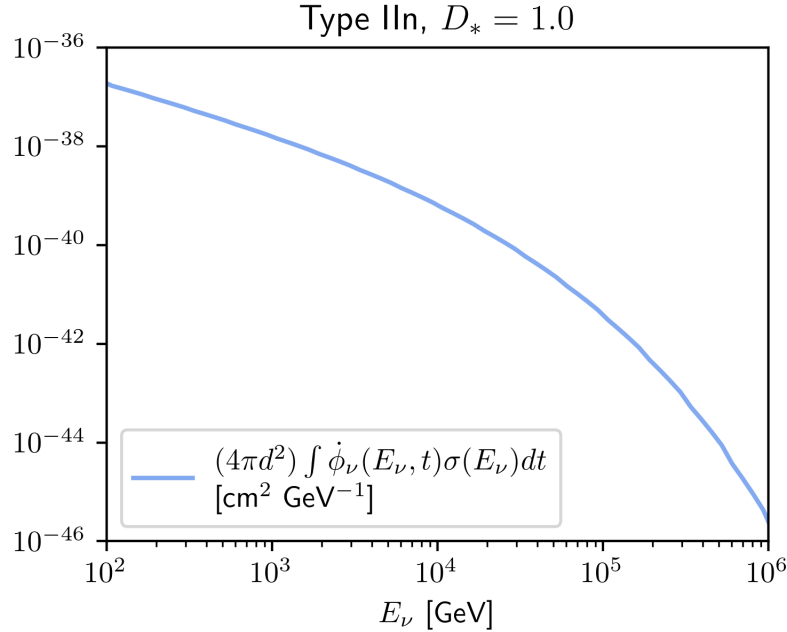
Channel	1	2	3
Signal	Hadronic shower	Hadronic shower + muon	Hadronic shower + Hadronic shower
Physical processes	All NC events	ν_μ CC events	ν_τ CC events + τ hadronic decay
	ν_e CC events	ν_τ CC events + $\tau \rightarrow \mu$ decay	
	ν_τ CC events + $\tau \rightarrow e$ decay		

Simulation of throughgoing events

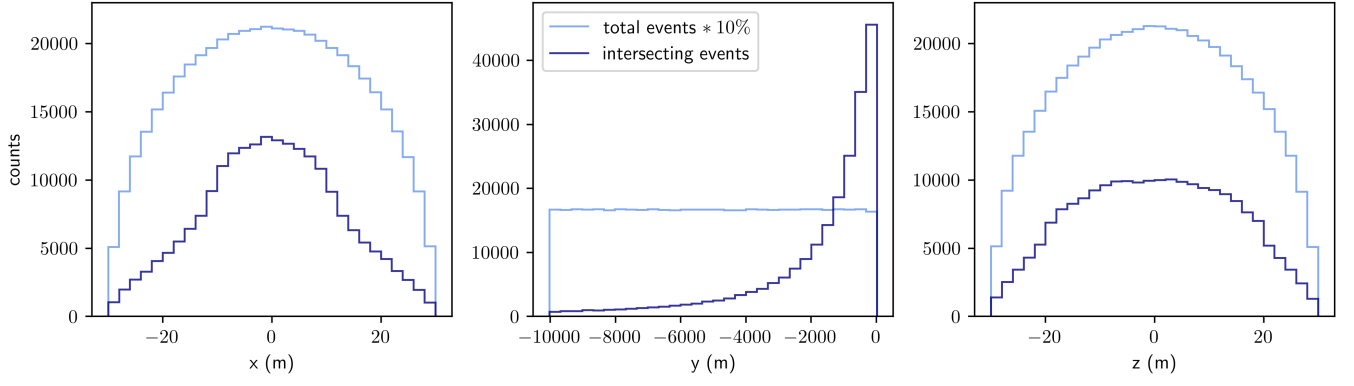
As explained in the text, throughgoing events are estimated with a Monte Carlo method using techniques described in Ref. [66]. First, a large number N'_{sim} of neutrino interaction vertices is generated uniformly in a cylindrical rock column with density $\rho_{\text{rock}} = 2.65 \text{ g cm}^{-3}$ resembling earth's crust, of dimensions 10 km length and 30 m radius with ATLAS at one end. Muons are thus exposed to a detector footprint of dimensions diameter \times length = $22\text{m} \times 40\text{m}$. These vertices are generated according to a neutrino energy distribution $(4\pi d^2) \int \dot{\phi}_\nu(E_\nu, t) \sigma_{\nu-\text{nuc}}(E_\nu) dt = \int \frac{dN_\nu}{dE_\nu dt}(E_\nu, t) \sigma_{\nu-\text{nuc}}(E_\nu) dt$, with the appropriate ϕ_ν and integration time for each SN scenario. An plot of this density is shown in Suppl. Fig. 1, for the example case of a Type IIIn, $D_* = 1.0$, SN.

This event generation process is done using **LeptonInjector** [66], which, after vertex-generation, samples the energy of the out-going muon from differential cross sections, and records only the muons which point in a direction that intersects the detector volume. Muons that intersect the detector volume are then propagated using **PROPOSAL** [67] until they reach a low-energy threshold on the scale of the muon mass. **PROPOSAL** considers both stochastic and continuous muon energy losses. Muons energetic enough to reach the detector are recorded and are considered part of the throughgoing signal, of which there are n events.

The physical event number is estimated by calculating the total number of interaction vertices expected in the rock using Eq. (1) and scaled by a factor n/N'_{sim} . Since the bulk of neutrinos considered ($\sim 90\%$) are below 10^4 GeV (see Fig. 2 (top)), we ignore the neutrino attenuation through Earth since it is known to be small at these energies [86].



SUPPL. FIG. 1. *Example (and un-normalized) energy distribution used for event generation.* $(4\pi d^2) \int \dot{\phi}_\nu(E_\nu, t) \sigma_{\nu-\text{nuc}}(E_\nu) dt$ with $\dot{\phi}_\nu$ corresponding to a SN IIIn, $D_* = 1.0$ SN scenario.



SUPPL. FIG. 2. ***Positions of vertices generated using *LeptonInjector*.*** The neutrino CC interaction vertices plotted in each spatial coordinate, uniformly distributed in a cylinder of radius 30 m and length 10 km; this cylinder lies along the y-axis. ATLAS is treated as a barrel-shaped detector with the beam axis along the z-axis. The light blue lines correspond to all N'_{sim} vertices generated (counts scaled by 0.1) and the dark blue lines correspond only to vertices with a muon that intersects the detector.